eprints@whiterose.ac.uk
https://eprints.whiterose.ac.uk/

Structural Control
and Health Monitoring
WILEY

Feasibility of shape memory alloy in a tuneable mass damper to reduce excessive in-service vibration

SCHOLARONE™
Manuscripts

1
2
3
4
5
6
7
8
9
10
11
12
13
14
15
16
17
18
19
20
21
22
23
24
25
26
27
28
29
30
31
32
33
34
35
36
37
38
39
40
41
42
43
44
45
46
47
48
49
50
51
52
53
54
55
56
57
58
59
60

Feasibility of shape memory alloy in a tuneable mass damper to reduce excessive in-service vibration

Haoyu Huang[a], Wen-Shao Chang[a,c], Khalid M. Mosalam[b]

[a] Department of Architecture and Civil Engineering, University of Bath, Bath, UK

[b] Department of Civil and Environmental Engineering, University of California, Berkeley, CA, USA

[c] Corresponding author, wsc22@bath.ac.uk

Abstract

The applications of shape memory alloy (SMA) in vibration reduction are benefited by its superelasticity and thermomechanical properties. This study is a part of a series of research projects focused on reduction of timber floor vibration. In this study, the feasibility of this tuneable mass damper is tested for in-service vibration reduction. At first, the effect of temperature ranging from 11°C to 120°C on the dynamic characteristics of SMA was investigated under different pre-stressed levels. At higher temperatures, the damping ratio reduces whilst stiffness increases, and vice versa with decreasing temperature. SMA is sensitive to temperature when the pre-stressed level is near the phase transformation stress. Next, the analytical model of timber floor system was built and idealised as a 2-degree-of-freedom system. Thirdly a series of lab tests were carried out and a damper consisting of an SMA bar was added on a cantilever beam with different natural frequencies, which represents floor system in the model. The results show that the vibration response of the system can be significantly reduced by the damper developed in this project, when the damper has resonance with the system. The mass of the system was then changed so as to make the damper out-of-tuned; the damper was then re-tuned by cooling/heating on SMA. After retuning of the damper, the response of the system was effectively reduced, which demonstrates the effectiveness and feasibility of employing SMA in the damper system.

Keywords

Shape memory alloy, Cu-Al-Mn, Tuned mass damper, Vibration reduction, In-service vibration

1 Introduction

Structural in-service vibration is a common behaviour which can be excited by both natural and human factors. Excessive floor vibration is an important serviceability issue generally caused by human activities like dancing and walking or the utilisation of machinery, especially when more economic construction materials and more light-weight elements are employed in timber engineering [1-3]. The vibration amplitude is much higher when the frequency of periodic forces is equivalent with the structural frequency, i.e. resonance occurs. To mitigate the vibration, tuned mass damper (TMD) installed on the floor systems served as an energy dissipater is studied [4-6], above all, designing less bulky damper still needs more research. This paper presents a part of a series of research focused on reducing timber floor vibration; as seen in Figure 1, in this project, a tuned mass damper using bending shape memory alloy (SMA) is developed. This TMD system is able to be space-efficient compared with TMD using tensile components and it can be placed between the beams, also, it aims to be active-tuneable.
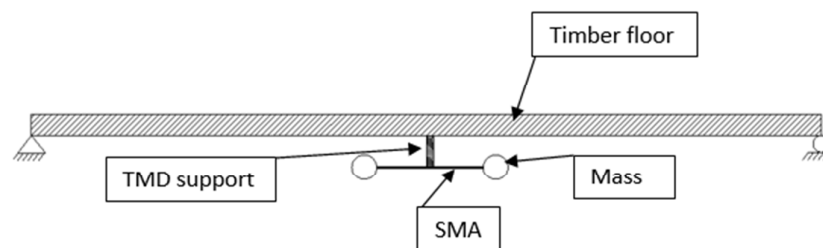
Figure 1 Timber floor using tuned mass damper by bending SMA

Shape memory alloy is a smart material and has been used in the medical industry, and mechanical and civil engineering sectors. SMA has superior mechanical characteristics compared to conventional materials, such as large recoverable deformation, high damping capacity and solid-solid phase transformation ability [7-11].

Two unique engineering characteristics of SMA are defined as superelasticity and shape memory effect (SME), which is shown in Figure 2. The shape memory effect is the ability of the alloys to revert to their initial shape upon heating until they enter their phase transformation temperature. Superelasticity is the ability of the alloys to experience comparatively large recoverable strains.
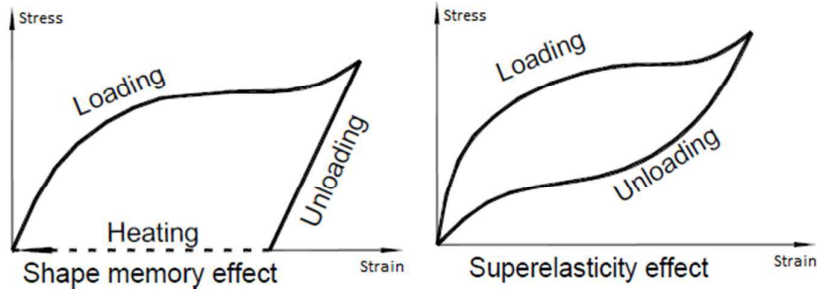
Figure 2 Stress-strain curve demonstrating the shape memory effect (left); superelasticity (right)
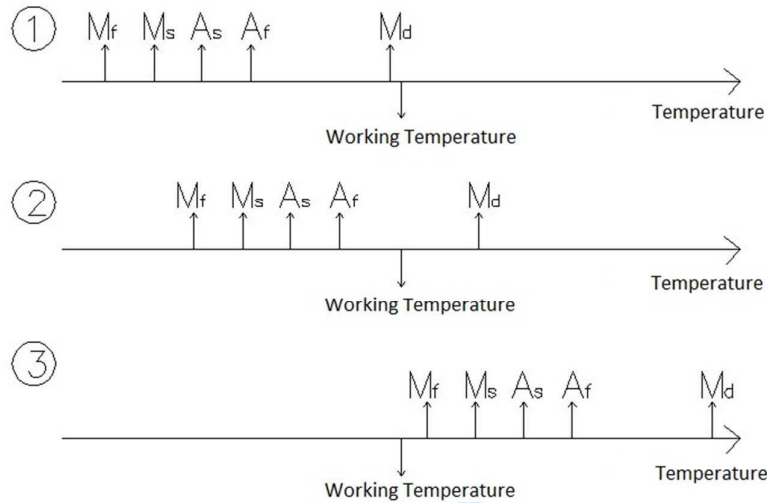
Figure 3 (1) Plastic deformation; (2) superelasticity; (3) shape memory effect

Because SMA is a solid-solid phase transformation material, the phase state depends on several different temperature levels. The phase transformation temperatures are the intrinsic properties of SMA represented by M_s, M_f, A_s and A_f in Figure 3, which stand for the start and finish (end) temperatures of martensitic and austenitic transformation, respectively. The deformation is superelastic when the working temperature is between A_f and M_d if the latter is above those four temperatures mentioned, and M_d indicates the maximum temperature required to induce superelastic deformation [12]. The superelasticity property decays when the working temperature approaches M_d and completely vanishes at temperatures above M_d, working temperature should be below M_f for the shape memory effect to take place. Earlier works on this topic can be found in [13, 14].

The sensitivity of SMA to temperature is a potential for applications, as shown in the studies by Araya, Marivil [15], Dolce and Cardone [16] and Andrawes and DesRoches [17]. They demonstrated that the transformation stress increases with the rise of the working temperature, which leads to the increase in stiffness. Shaw and Kyriakides [18] indicated the strong dependence of the stress-strain

curve of superelastic SMA on temperature results first in the decrease of the equivalent damping ratio with increasing temperatures. However, the equivalent damping ratio starts to increase around and above temperature M_d, i.e., when the superelasticity decays and vanishes. SMA therefore is able to exhibit different deformation forms through adjusting temperature states.

SMAs have been used to reduce vibration, due to their superelasticity and high energy dissipation capacity. Therefore, satisfactory fatigue working life is of importance; SMA material characterisations regarding to fatigue-fracture and damping evolution were studied and the enhancement of stability was discussed [19-24]. Pre-training before the application is a solution to obtain a stable behaviour so as to reduce the influence of stabilisation [16]. The SMA-based vibration reduction systems can be classified into passive and active controls. When SMAs are used in a passive control system, superelastic and high damping capacity are utilised. Several researchers have developed SMA-based energy-absorption devices which generally consist of SMA wires [25-30]. These devices provide high damping and recentering capacity, and can be easily installed in the main structures to increase damping.

Along with the trend for in-service adaptability in engineering, SMA is becoming a popularly investigated material as it can provide active control functions by its particular thermomechanical properties [31, 32]. For active vibration control, the SME property of SMA is frequently used to actuate the system by its thermal activation [11, 32, 33]. When the martensitic SMAs are heated, they will recover their initial shape (temperature-induced transformation) and the recovering force can be used as a mechanical stroke for actuation. The requirement of this application is that the heating/cooling cycle on SMAs should be fast; otherwise the effectiveness of active control would be reduced.

Another way to use SMAs in active control systems is referred to semi-active control in which the physical or mechanical properties are changed by an external actuation. SMA can be used to re-tune the frequency to change the main structural frequency. Liang and Rogers [31] heated NiTi SMA springs by a power supply and observed the variation in the spring constant, enabling the system to control the vibration. Williams, Chiu [34] used SMA in a tuned mass damper attached to a cantilever beam. By changing the stiffness of SMA using different heating combinations, it was observed that the vibration can be attenuated for several discrete frequencies. Rustighi, Brennan [35] developed an active tuned mass damper system and found that temperature control of SMAs can control the frequencies of the damper within a limited range. The aforementioned temperature active control approach using SMA was developed so as to reduce the machine-induced vibration with a specific known frequency to be tuned; however, in a building structure the in-service vibration often involves

4

a wide range of frequencies. This paper aims to implement Cu-Al-Mn SMA in a tuned mass damper and optimise its effectiveness by varying stiffness and damping of the SMA.

2 Dynamic characteristics of SMA under different temperature and pre-stressed levels

Cu-Al-Mn SMA is selected to test in this study as copper has much higher thermal conductivity compared with other metals (nickel and titanium), which is efficient to keep the inner temperature and surface temperature of SMA bar consistent. It is important that copper-based SMA costs less money, therefore has the potential for civil engineering applications regarding to its large demand [36, 37]. In addition, the development of Cu-Al-Mn SMA in civil engineering is underway in recent years [9, 36, 38-40]. In this study, the dynamic modulus and damping of Cu-Al-Mn SMAs were tested at different temperatures and pre-stressed levels, since these dynamic characteristics may vary with the variation of the pre-stressed levels because of phase transformation.

2.1 Experimental methods

A superelastic Cu-Al-Mn (Cu = 81.84%, Al = 7.43% and Mn = 10.73% by weight) bar with a diameter of 12 mm and length of 125 mm was used in this study, which was provided by Furukawa Techno Material Co., Ltd., Japan. The phase transformation temperatures are $M_s = -74°C$, $M_f = -91°C$, $A_s = -54°C$ and $A_f = -39°C$, so superelastic deformation occurs at room temperature. The SMA used is a polycrystalline material and the grain size is 54 mm. The SMA bar was machined so as to have a rectangular section in the middle with a dimension of $10×3$ mm^2 and the effective length for vibration was set to be 50 mm as shown in Figure 4 (a). This rectangular- section zone is the effective zone.
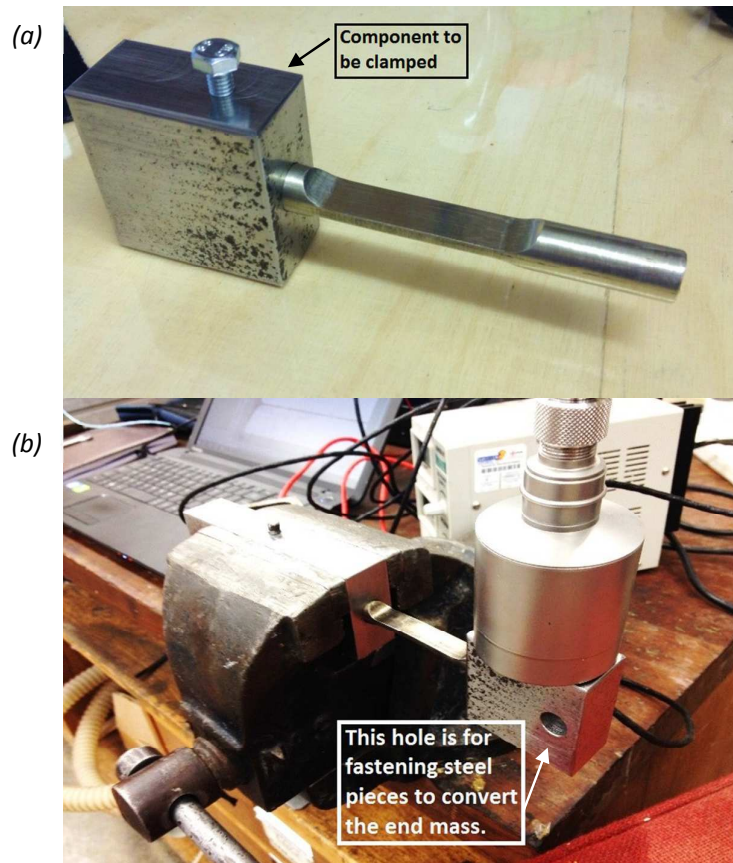
Figure 4 (a) Cu-Al-Mn SMA vibration sample; (b) SMA free vibration test set-up

The SMA sample was tested as a cantilever beam under free vibration as shown in Figure 4 (b). A constant force of about 14 N was applied to the cantilever beam by hanging a steel block to initiate the displacement in each test and free vibration was generated after the force was removed. The acceleration was measured by an accelerometer attached to the cantilever beam at a sampling rate of 100 Hz for a duration of one minute.

The experimental tests were conducted under different pre-stressed levels in order to examine the sensitivity to temperature under different pre-loading conditions. The pre-stressed levels were set by the weights fastened through the hole on the steel block (Figure 4 (b)). Different loads have been selected as 13.1 N, 21.7 N, 35.7 N and 52.7 N to provide different pre-stressed levels of 79 MPa, 131 MPa, 216 MPa and 319 MPa at the end of effective zone on clamping side. The pre-stressed levels presents the maximum stress (at the location of surface) calculated using the product of the bending moment and the distance from the neutral axis divided by the area moment of inertia. These loads lead to corresponding strain values of 0.30%, 0.47%, 1.21% and 3.04%. The strain values were tested by strain gauge at the location where the pre-stress values are calculated, and the static loading strain-stress curve can be estimated in Figure 5. From Figure 5, the transformation strain is at about

6

1%, which has also been found in our previous materials studies. It can be observed that the pre-stressed levels at 216 MPa and 319 MPa can induce nonlinear deformation and SMA is under stress-induced transformation from austenite to martensite.

In each pre-stressed level, the SMA beam was tested under free vibration at a wide range of temperatures (11°C, 17°C, 21°C, 50°C, 80°C and 120°C). To reach 11°C and 17°C, the SMA beam was cooled down by surrounding ice cubes. SMA was heated by wrapping energised carbon fibre. The high temperature levels can be controlled and stabilised by adjusting voltage and current controlled by a DC power supply. During the cooling/heating, the surface temperature was measured by an infra-red thermometer. Even though copper-based SMA has high thermal conductivity, 2-minute extra heating and cooling were done to make sure inner temperature reaches expected value. Under each pre-stressed testing condition and temperature condition, three tests were repeated to evaluate the statistical variations.
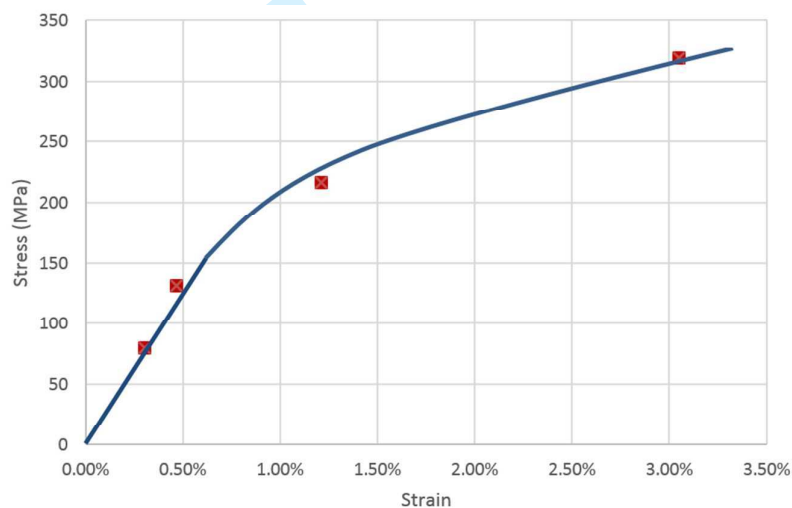
Figure 5 Static strain-stress graph of SMA cantilever beam

2.2 Results

The data recorded was analysed to obtain the natural frequency and damping ratio. In the analysis, linear-prediction SVD (singular-value decomposition) -based Matrix Pencil method (MP), summarised by Zieliński and Duda [41] and proposed by Sarkar and Pereira [42], was applied to compute the natural frequency and damping ratio. The MP approach is a computationally efficient and precise method producing a small variance.

The MP approach aims to deal with the approximation for complex exponentials in the signal. The observed signal is modelled as Equation (1):

7

$$y(kT_s) \approx \sum_{i=1}^{M} R_i z_i{}^k + n(kT_s) \tag{1}$$

$$z_i = e^{(-\alpha_i + j\omega_i)T_s} \tag{2}$$

where $y(kT_s)$ is the noise-contaminated signal, R_i is the amplitude, T_s is the sampling period, kT_s is the time duration, $n(kT_s)$ represents the noise, and M is the estimated number of complex exponentials. In Equation (2), α_i and ω_i are damping factor and angular frequency, respectively and $j = \sqrt{-1}$. By using the MP approach, z_i can be solved based on SVD.
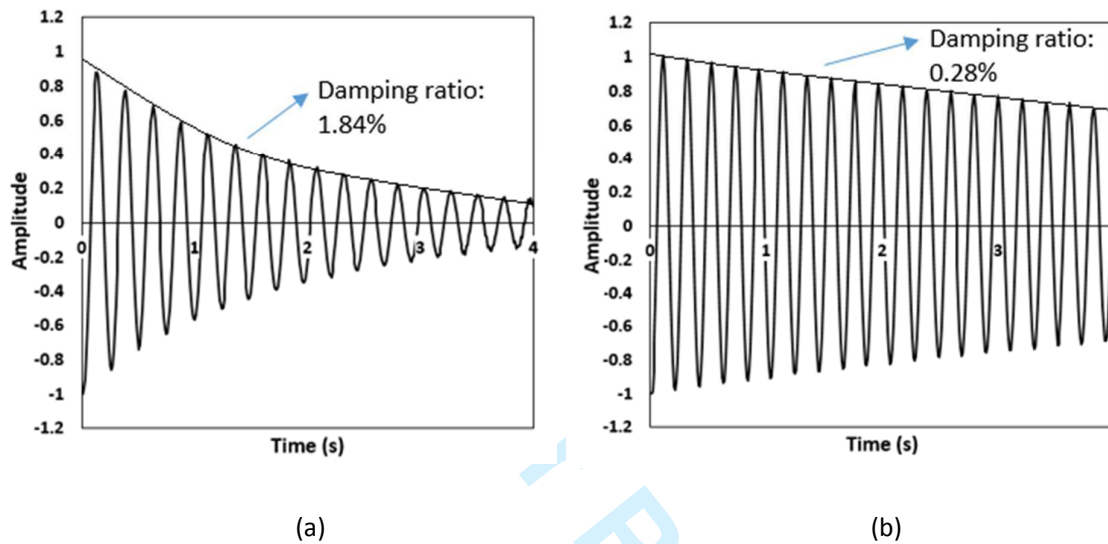
(a)

(b)

Figure 6 Normalised free vibration response at pre-stress level of 216 MPa in first 4 seconds (a) at 11 ℃; (b) at 80 ℃

Figure 6 shows the free vibration at the pre-stress level of 216 MPa in first 4 seconds in comparison between 11℃ and 80℃ which are the two temperatures considered reasonable in the applications. For comparison, the acceleration data in Figure 6 (a) are normalised to 0.29 and those in Figure 6 (b) are normalised to 0.86. It can be observed that the vibration frequency is higher at 80℃, and the damping is higher at 11℃. The effects of the temperature on the natural frequency of the SMA cantilever beam at pre-stressed level of 216 MPa are presented in Figure 7. From the tests, the natural frequency decreases with the increase in the pre-stressed levels and decrease in the working temperature. On the other hand, the natural frequency of the SMA beam shows higher dependency on the pre-stressed levels than on the temperature, which implies that changing the mass attached to the beam is a more efficient way to adjust the natural frequency. The equivalent stiffness depends on temperature and pre-stress levels. From Figure 8, the stiffness increases with the increase of temperature. In the tests, it is found the stiffness of SMA beam with pre-stressed levels of 79 MPa and 131 MPa increased by 10.7% and 17.3% when the working temperature was

increased from 11°C to 120°C, respectively. The transformation stress is highly sensitive to temperature and the stiffness can be influenced by temperature significantly at higher pre-stressed levels. However, for the higher stress level of 319 MPa the change is not significant, because stiffness increases when the SMA is cooled down to 11°C. This behaviour can be explained by the fact that SMA may have deformed in martensitic elastic state. As presented by Gencturk, Araki [43], after loading to 6% strain, Cu-Al-Mn SMA is in martensitic elastic state and the stiffness starts to increase.
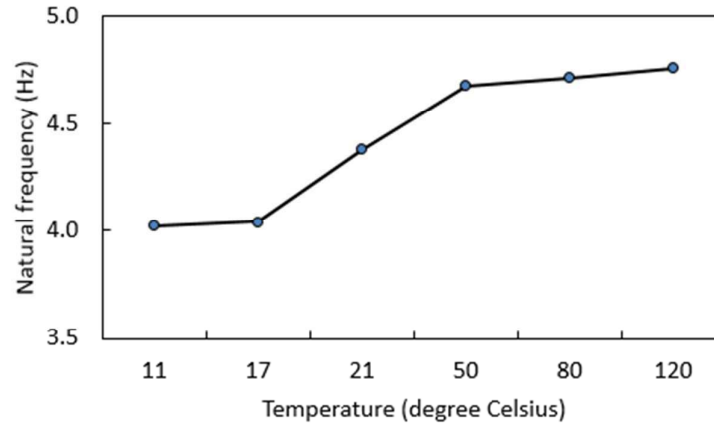
Figure 7 Effect of temperature on the natural frequency of SMA cantilever beam at pre-stress level of 216MPa

Figure 8 Effect of temperature on the equivalent stiffness of SMA cantilever beam at pre-stress level of 216MPa

9
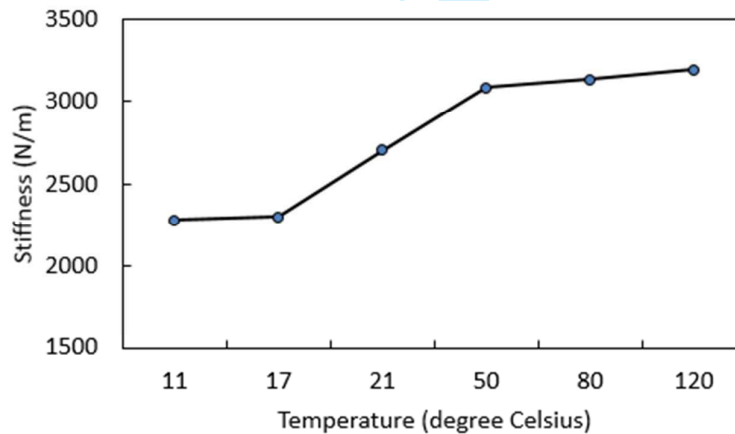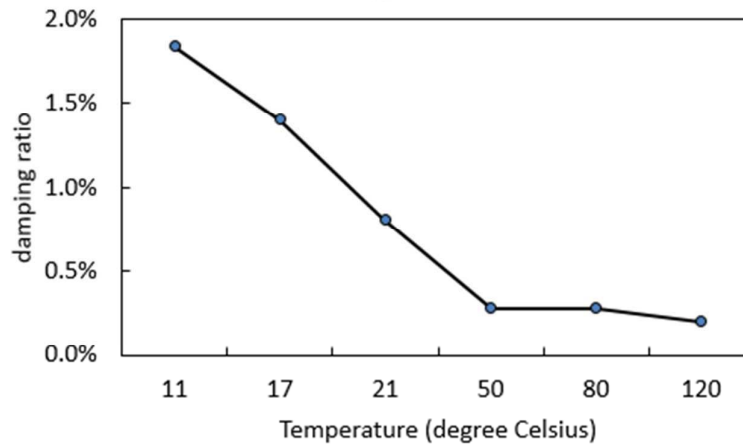
In Figure 9, the damping ratio is higher at lower temperatures. From the tests, it is also observed that a higher pre-stressed level can dissipate more energy since the SMA deforms in the nonlinear range. Under 216 MPa pre-stressed level, the damping ratio can be changed most significantly, from 1.84% at 11°C to 0.20% at 120°C as shown in Figure 9. When the SMA is cooled down, the transformation stress can be lowered and the SMA can be easily transformed to martensite. This test shows that the SMA is more sensitive to temperature when the pre-stress level is near the phase transformation starting stress due to the fact that the deformation can be transformed easily between linear and nonlinear ranges by changing the temperature.

2.3 Discussion

Previous research has shown the same trend as observed in this study; higher temperature leads to higher stiffness and lower damping capacity. However, higher temperature above the range of this test could result in an increase in both damping ratio and stiffness [12, 18].

Torra, Isalgue [44] reported that temperature affects the stiffness and damping of both copper-based SMA and NiTi-based SMA but that the dependency differs, and this can also be evidenced by works from Strnadel, Ohashi [45] and Araya, Marivil [15]. The rate which describes the relationship between temperature and stress is called the Clausius-Clapeyron coefficient (C-C slope). The results of Torra et al. (2004) show the C-C slope of NiTi alloy is 6 times more than that of the Cu-Al-Be. Niitsu, Omori [46] indicated that the C-C slope for Cu-Al-Mn SMA was 2.7 MPa/°C in their tests, and Nemat-Nasser, Choi [47] estimated the NiTi SMA C-C slope was 6 MPa/°C. Therefore, it can be concluded that the growth of transformation stress leading to increase in stiffness, with temperature of NiTi-based SMA is larger than that of copper-based SMA. For precise adjustment using temperature, if the C-C slope is large, it is difficult to adjust to the target stress exactly, as high

precision of temperature control is hard to achieve. In this case, copper-based SMA is more appropriate than NiTi. However, for the purpose of increasing the stress by a large margin within a short time, NiTi exhibits a better performance. Copper-based SMA and NiTi SMA can therefore play different roles in active control. Moreover, how to develop a system to control temperature via heating and cooling will be a next step. In the future, more efficient and more applicable cooling method such as 1,1,1,2-tetrafluoroethane cooling system will be developed.

The results of dynamic characteristics are calculated from a free vibration generated by a specific initial force, and the initial force is selected based on the measurement range of accelerometer and tools in the lab. It is important to bring out that stiffness values and damping values are amplitude-dependent, especially damping depends on the hysteresis. The damping ratio (ξ) has the relationship as seen in the equation: $\xi = \Delta W/(4\pi W)$, in which ΔW is the dissipated energy, and W is the equivalent elastic strain energy [48]. Therefore, stiffness and damping values are changeable with the hysteretic curve and the specific values should be further studied in real time in order to determine the amplitude dependence. In this test, the dynamic characteristics are averaged values form a one-minute free decaying wave including different amplitudes.

3 Application of SMA to tuned mass damper

3.1 Fundamentals of tuned mass damper

Tuned mass damper (TMD) is a less-complicated device for structural response reduction in respect of its easy installation on structures. TMD is a device consisting of a spring, damper and mass [49]. The function of TMD is that its natural frequency can be tuned to a particular frequency to match the main structure, so the damper can resonate with the structure. The motion of TMD is a way of outputting energy; thus the energy input in the structure can be dissipated and the vibration can be mitigated.

Figure 10 Idealisation of the timber floor system with TMD

11
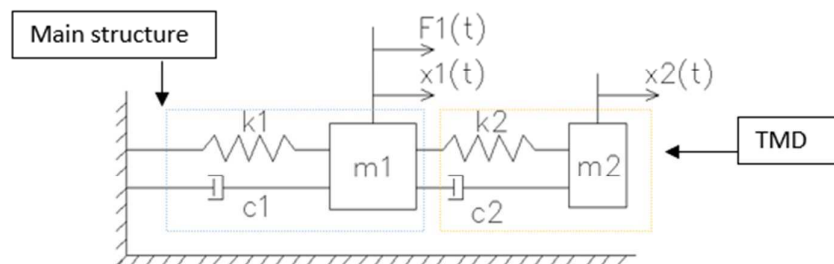
Figure 10 is an idealisation of the timber floor system with TMD (Figure 1) to describe the behaviour. m_1 represents the concentrated mass of the floor and m_2 implies the mass of the TMD, k_1, k_2 and c_1, c_2 stand for the stiffness and damping of the main structure and the TMD, respectively, F_1 is a dynamic excitation load on the main structure modelling structural in-service vibration, and x is the corresponding displacement, with superposed dots implying derivatives with respect to time.

For each free body, the equations of motion can be input to the matrix.

$$\begin{bmatrix} m_1 & 0 \\ 0 & m_2 \end{bmatrix} \begin{bmatrix} \ddot{x}_1 \\ \ddot{x}_2 \end{bmatrix} + \begin{bmatrix} c_1 + c_2 & -c_2 \\ -c_2 & c_2 \end{bmatrix} \begin{bmatrix} \dot{x}_1 \\ \dot{x}_2 \end{bmatrix} + \begin{bmatrix} k_1 + k_2 & -k_2 \\ -k_2 & k_2 \end{bmatrix} \begin{bmatrix} x_1 \\ x_2 \end{bmatrix} = \begin{bmatrix} F_1 \\ 0 \end{bmatrix} \tag{3}$$

which can be generalised as:

$$\begin{bmatrix} m_{11} & m_{12} \\ m_{12} & m_{22} \end{bmatrix} \begin{bmatrix} \ddot{x}_1 \\ \ddot{x}_2 \end{bmatrix} + \begin{bmatrix} c_{11} & c_{12} \\ c_{12} & c_{22} \end{bmatrix} \begin{bmatrix} \dot{x}_1 \\ \dot{x}_2 \end{bmatrix} + \begin{bmatrix} k_{11} & k_{12} \\ k_{12} & k_{22} \end{bmatrix} \begin{bmatrix} x_1 \\ x_2 \end{bmatrix} = \begin{bmatrix} F_1 \\ 0 \end{bmatrix} \tag{4}$$

Assume the external force is harmonic.

$$F_1 = F_0 e^{j\omega t}, x_1 = X_1 e^{j\omega t}, x_2 = X_2 e^{j\omega t}$$

The matrix becomes:

$$\begin{bmatrix} -\omega^2 m_{11} + j\omega c_{11} + k_{11} & -\omega^2 m_{12} + j\omega c_{12} + k_{12} \\ -\omega^2 m_{12} + j\omega c_{12} + k_{12} & -\omega^2 m_{22} + j\omega c_{22} + k_{22} \end{bmatrix} \begin{bmatrix} X_1 \\ X_2 \end{bmatrix} = \begin{bmatrix} F_0 \\ 0 \end{bmatrix} \tag{5}$$

Let $z_{mn}(\omega) = -\omega^2 m_{mn} + j\omega c_{mn} + k_{mn}$

$$\begin{bmatrix} z_{11}(\omega) & z_{12}(\omega) \\ z_{12}(\omega) & z_{22}(\omega) \end{bmatrix} \begin{bmatrix} X_1 \\ X_2 \end{bmatrix} = \begin{bmatrix} F_0 \\ 0 \end{bmatrix} \tag{6}$$

$$[Z] \begin{bmatrix} X_1 \\ X_2 \end{bmatrix} = \begin{bmatrix} F_0 \\ 0 \end{bmatrix} \text{ and } \begin{bmatrix} X_1 \\ X_2 \end{bmatrix} = \begin{bmatrix} F_0 \\ 0 \end{bmatrix} [Z]^{-1} \tag{7}$$

Let $[H] = [Z]^{-1}$

$$\begin{bmatrix} X_1 \\ X_2 \end{bmatrix} = \begin{bmatrix} F_0 \\ 0 \end{bmatrix} [H] \tag{8}$$

Therefore, a typical frequency response of the structure -TMD system can be drawn by $X_1 = H_{11}F_0$ for the main structure and $X_2 = H_{21}F_0$ for the TMD. As an example given by Schmitz and Smith [50], when a damper is added to a Single Degree of Freedom (SDOF) system, the amplitude of vibration is significantly reduced at the natural frequency of the main structure as the damper can resonate. The

12

performances of TMD in civil structures were studied and the optimal design methods were developed [51-53].

The drawback of the TMD is that it is sensitive to the change of the main structure and is easily out-of-tune [54] so that subsequently its effectiveness is significantly reduced. In practice, the natural frequency of building structures can be easily affected by environmental conditions (analogous to how the exterior building environment changes by date), damage due to extreme events, such as earthquakes, and increase/reduction of mass [55-58]. Thus, it is vital to adjust the natural frequency of the TMD actively, thereby tuning the structure effectively.

3.2 Experimental investigation

As explained previously, the most effective way to resolve the issue of off-tuning of a TMD system is to change the mass of the system. However, this is not always easy, particularly when the system is already installed. To demonstrate the potential of change in working temperature of the TMD employing an SMA beam for active control, this study uses a Cu-Al-Mn SMA beam with a mass attached as the TMD to reduce the vibration of a SDOF system, as shown in Figure 11. A cantilever beam made of mild steel with section of 100×10 mm^2 and 520 mm in length was designed with adjustable mass attached to the free end. Another cantilever beam made of Cu-Al-Mn SMA with section of 10×3 mm^2 and effective length of 50 mm was used as the TMD. At first, a mass was hung at the end of the steel beam using string and the free vibration was triggered by cutting off the string. The resulting accelerations were measured by accelerometers. The experimental sequences and factors are tabulated in Table 1. The ambient temperature of the laboratory was 21℃, and each test combination was repeated three times to ensure consistency of results. In this series of tests, the mass of the TMD does not change and the natural frequencies of the TMD system are controlled by a change of working temperature which, as previously discussed, leads to changes in the stiffness and damping properties of the system.

13
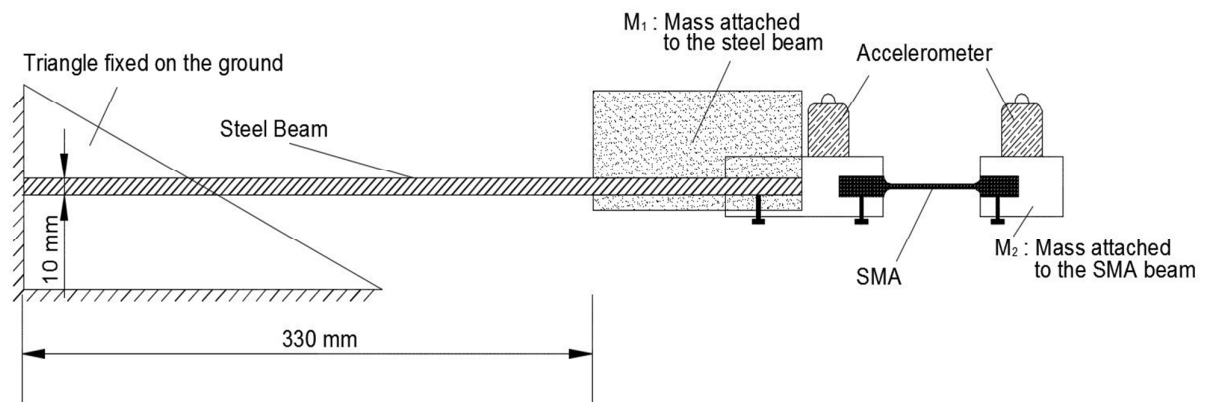
Figure 11 Schematic drawing of the experimental set-up

Test No. 2 keeps $k_1/m_1 = k_2/m_2$ so the TMD system was in nearly-optimised condition. The mass of the main structure was increased in Test No. 4, representing the change of use for the main structure; the TMD was then off-tuned and became less effective. The SMA beam in TMD was then cooled down to 11°C to retune the main structure in Test No. 5. The mass in the main structure was then reduced to 54.1 kg which lead to the TMD being off-tuned again in Test No. 7, followed by the SMA beam being heated to 120°C to retune the main structure in Test No. 8.

3.3 Comparison

From the free decaying data in each test, the damping ratio and natural frequency can be computed by using the MP approach described previously. Figure 12 presents the comparison between the response before and after installing the TMD when $m_1 = 61.6$ kg. In this case, the natural frequency of the damper is tuned to be nearly equal to that of the beam so that the response can be significantly reduced at about 4.4 Hz. Two modes appear after adding the damper and the highest response is still much lower than the previous, which is in line with the results demonstrated by Schmitz and Smith [50].
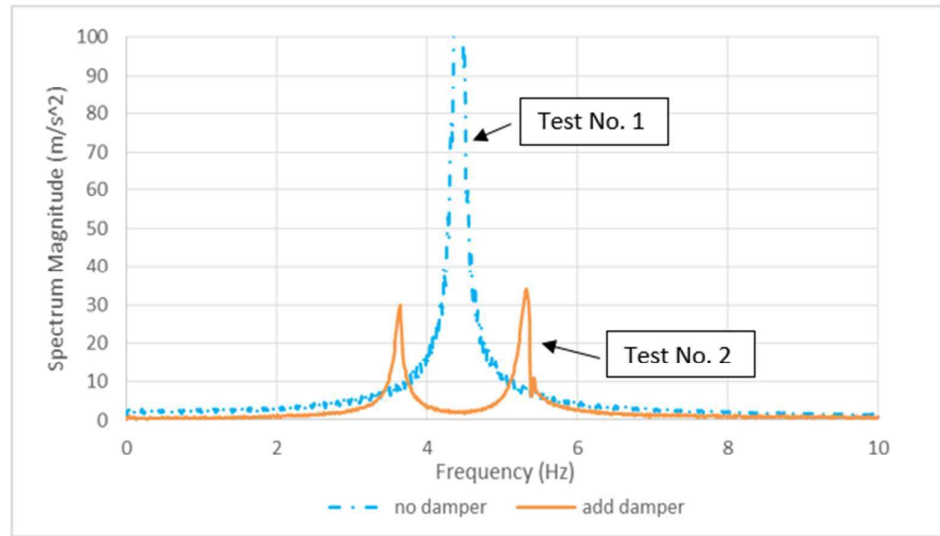
Figure 12 Frequency response of cantilever beam without and with damper ($m_1 = 61.6\ kg$)
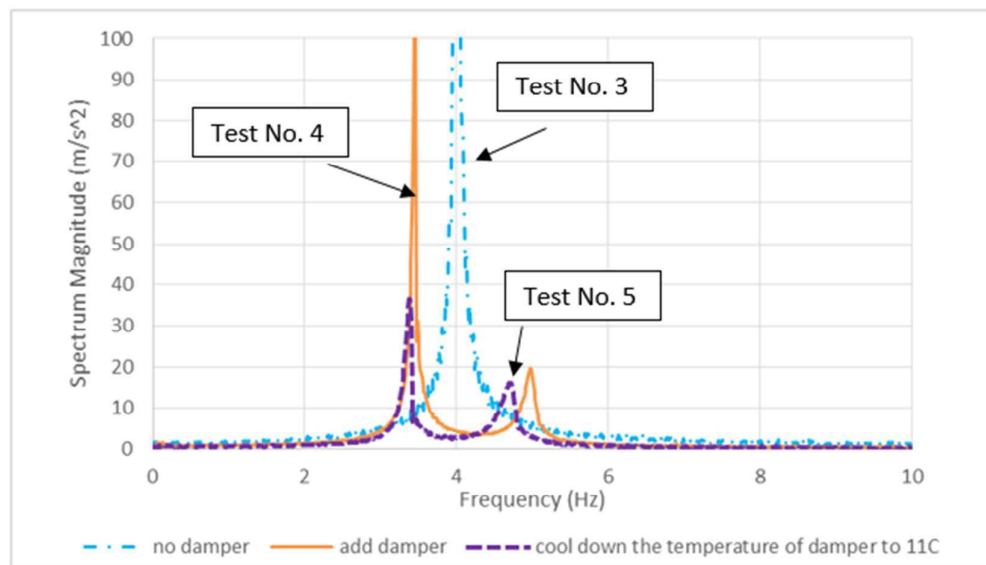
Figure 13 Frequency response of cantilever beam without damper, with damper and with temperature controlled damper ($m_1 = 71.5\ kg$)

The results of Tests Nos. 3, 4 and 5 are summarised in Figure 13. When the mass of the main structure changes, the TMD becomes off-tuned, as shown in Figure 13, and the first mode of the structure moves to the lower frequency region where there is a spike. When the SMA beam in the TMD is cooled down to 11°C, the spectrum magnitude is significantly reduced particularly in the first mode.

Figure 14 compares the test response spectra of Tests Nos. 6, 7 and 8, where the mass of the main structure was decreased to 54.1 kg and the natural frequency of the main structure without the

15

TMD was increased to 4.74 Hz. The system with the original TMD (Test No. 7) appears to be off-tuned; test No. 8 represents the response of the whole system with the TMD being heated to 120°C. As shown in Figure 14, the response can be reduced in the range between 4.3 Hz and 5.6 Hz, but the response in the first and second modes is even increased. The reason is that the damping capacity of the SMA at 120°C is low. For vibration reduction through heating the SMA, only a narrow frequency band near the structural resonance frequency can be controlled. To control a broader frequency band, it is less appropriate to increase the temperature of SMA due to the fact that SMA would not provide enhanced damping.
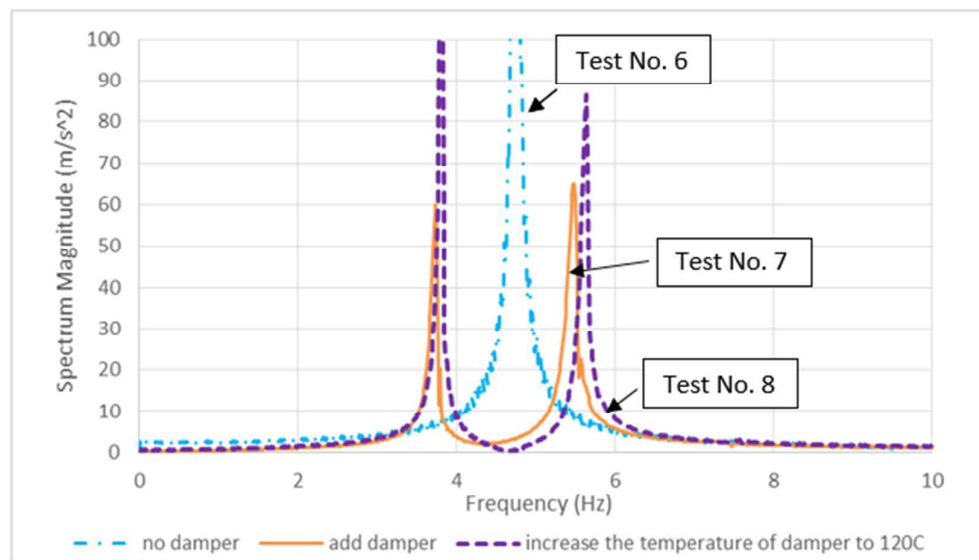
Figure 14 Frequency response of the cantilever beam without damper, with damper and with temperature controlled damper ($m_1 = 54.1 \ kg$)

3.4 Discussion

Williams, Chiu [34] reported that to control the vibration by using TMD, the excitation frequency is discrete and should be known in advance. However, for applications in buildings during in-service vibration, the excitation frequency is in a wide range. The vibration reduction should be effective in a wider frequency band around the natural frequency of structure.

Increasing the working temperature of SMA can lead to higher stiffness but lower damping ratio, which is effective to control the vibration in a narrow range, e.g. the vibration induced by machines. The target for optimisation, in this case for building structural applications, is that both stiffness and damping ratio be increased so as to keep the response small. If the elements connected with the mass are in parallel and their motions have the same displacement and velocity, their stiffness and damping coefficient can be added together as in [59]:

16

$$K = K_1 + K_2 + \cdots + K_n \tag{9}$$

$$C = C_1 + C_2 + \cdots + C_n \tag{10}$$

K and C represent the total stiffness and damping coefficient of the SMA damper, K_i and C_i imply the corresponding properties in each element. The temperature adjustment on the SMA can be a combination and there could be a number of SMA elements in parallel, in which some are cooled down and some are heated up. Through the adjustment process, K can control the natural frequency of the TMD near the optimal value in order to increase resonance, while C is able to provide as much damping as a possibility to reduce the highest amplitude in the first and second modes. There will be a future research direction for SMA heating/cooling combinations.

As this study is a part of a series of research for floor vibration control as shown in Figure 1, the cantilever beam model in this paper requires scaling. Two practical limitations need to be compromised, and one of them is the mass ratio between the mass of TMD and the mass of floor, as the supplementary mass cannot be too heavy and the floor carrying capacity has to be assured. Another limitation is the relative motion of TMD, and it should be restricted in a safety range to protect the floor [60]. In the practical application to floor system, the size of SMA beam may need to be larger compared with the model in laboratory, therefore SMA properties such as stiffness, damping ratio and heat-transfer capacity should be concerned after scaling. The stiffness of SMA beam should meet the requirement that its natural frequency is able to tune the natural frequency of the primary structure. The damping ratio can be improved by increasing the number of SMA elements in parallel like aforementioned SMA combinations. As the heating is from surface to the inside, for larger size, higher electrical power may need in order to fully heat. To achieve precise control, the heating time will be estimated by simulation corresponding to the actual size.

Self-heating of SMA is an issue in dynamic applications [16, 18], and is commonly due to the latent heat during phase transformation [61]. The extra heat from self-heating influences the shape of the hysteresis loops thus changes the fracture level of SMA. With regard to the timber floor application, the free vibration is common. Therefore, the solution to reduce the self-heating is to increase more damping so as to dissipate more energy, attenuate the vibration faster and reduce the cyclic deformations of SMA. In further SMA-based TMD design, the damping of SMA should be considered to be improved, for instance, multiple SMA elements can be employed in parallel.

17

4 Conclusion

As a part of a series of research focused on timber floor vibration, this paper studies the feasibility of a new TMD system using bending SMA. To apply SMA in structural in-service vibration reduction systems, the effect of temperature on the dynamic characteristics of SMA was studied and a TMD with a Cu-Al-Mn SMA beam was tested. The dynamic characteristics, such as stiffness and damping of Cu-Al-Mn SMA, were characterised by free vibration tests under different pre-stressed levels and temperatures. With the increase of temperature up to 120℃, the damping ratio decreases and stiffness increases. When the SMA is cooled down to 11℃, the damping ratio can be increased while the stiffness is reduced. The influence of temperature change is most sensitive when the pre-stressed level is near the transformation stress at 216 MPa for the studied case.

The floor vibration system was idealised as a 2-DOF model and the feasibility was tested using a cantilever beam. SMA was used as a means for stiffness and damping adjustment in TMD added on a cantilever beam, and at first this TMD was in the near optimal condition capable to tune the natural frequency of the beam. After increasing the mass clamped on the beam to disturb the tuning condition, the vibration response increased, but the response can be significantly reduced by cooling SMA as the new main structural natural frequency can be effectively tuned. When the mass on the cantilever beam is reduced, heating SMA can reduce the response at a narrow frequency band near the resonance frequency. It is not appropriate to reduce the response for a wider frequency range due to decreasing damping in the SMA. In future research, an optimisation needs to be studied regarding this case. Both cooling and heating can operate on a number of SMA elements and, after combination, an effective tuning frequency and enough damping capacity are expected to be achieved.

Acknowledgement

References:

1.   Weckendorf, J., *Dynamic response of structural timber flooring systems*, in *The Centre for Timber Engineering, School of Engineering and the Built Environment*. 2009, Edinburgh Napier University.
2.   Hu, L.J., Y.H. Chui, and D.M. Onysko, *Vibration serviceability of timber floors in residential construction.* Prog. Struct. Engng Mater., 2001(3): p. 228-237.

3. Smith, I., *Vibrations of timber floors: serviceability aspects*, in *Timber engineering*, S. Thelandersson and H.J. Larsen, Editors. 2003, Wiley Chichester. p. 241-266.

4. Webster, A.C. and R. Vaicaitis, *Application of Tuned Mass Dampers to Control Vibrations of Composite Floor Systems.* Engineering Journal-American Institute of Steel Construction Inc, 1992. **29**(3): p. 116-124.

5. Setareh, M. and R.D. Hanson, *Tuned Mass Dampers to Control Floor Vibration from Humans.* Journal of Structural Engineering-Asce, 1992. **118**(3): p. 741-762.

6. Setareh, M., et al., *Semiactive tuned mass damper for floor vibration control.* Journal of Structural Engineering-Asce, 2007. **133**(2): p. 242-250.

7. DesRoches, R. and B. Smith, *Shape memory alloys in seismic resistant design and retrofit a critical review of their potential and limitations.* Journal of earthquake engineering, 2003. **7**: p. 1 - 15.

8. Ozbulut, O.E., S. Hurlebaus, and R. Desroches, *Seismic response control using shape memory alloys: a review.* Journal of intelligent material systems and structures, 2011. **22**(14): p. 1531-1549.

9. Chang, W.S., et al., *Technical Note: Potential to Use Shape Memory Alloy in Timber Dowel-Type Connections.* Wood and Fiber Science, 2013. **45**(3): p. 330-334.

10. Cladera, A., et al., *Iron-based shape memory alloys for civil engineering structures: An overview.* Construction and Building Materials, 2014. **63**: p. 281-293.

11. Janke, L., et al., *Applications of shape memory alloys in civil engineering structures - Overview, limits and new ideas.* Materials and structures, 2005. **38**(279): p. 578-592.

12. Duerig, T.W., *Engineering aspects of shape memory alloys*. 1990, London ; Boston: Butterworth-Heinemann. xi, 499 p.

13. Pops, H., *Stress-Induced Pseudoelasticity in Ternary Cu-Zn Based Beta Prime Phase Alloys.* Metallurgical Transactions, 1970. **1**(1): p. 251-&.

14. Nakanishi, N., *Lattice softening and the origin of SME*, in *Shape Memory Effects in Alloys*, J. Perkins, Editor. 1975, Plenum press: New York. p. 305-326.

15. Araya, R., et al., *Temperature and grain size effects on the behavior of CuAlBe SMA wires under cyclic loading.* Materials science and engineering A - structural materials properties microstructure and processing, 2008. **496**(1-2): p. 209-213.

16. Dolce, M. and D. Cardone, *Mechanical behaviour of shape memory alloys for seismic applications - 2. Austenite NiTi wires subjected to tension.* International journal of mechanical sciences, 2001. **43**(11): p. 2657-2677.

17. Andrawes, B. and R. DesRoches, *Effect of ambient temperature on the hinge opening in bridges with shape memory alloy seismic restrainers.* Engineering structures, 2007. **29**: p. 2294 - 2301.

18. Shaw, J.A. and S. Kyriakides, *Thermomechanical aspects of NiTi.* Journal of the mechanics and physics of solids, 1995. **43**(8): p. 1243-1281.

19. Torra, V., et al., *Shape memory alloys as an effective tool to damp oscillations Study of the fundamental parameters required to guarantee technological applications.* Journal of Thermal Analysis and Calorimetry, 2015. **119**(3): p. 1475-1533.

20. Torra, V., et al., *Damping in civil engineering using SMA. The fatigue behavior and stability of CuAlBe and NiTi alloys.* Journal of Materials Engineering and Performance, 2009. **18**(5-6): p. 738-745.

21. Casciati, S. and A. Marzi, *Experimental studies on the fatigue life of shape memory alloy bars.* Smart Structures and Systems, 2010. **6**(1): p. 73-85.

22. Khan, M.I., et al., *Combined effects of work hardening and precipitation strengthening on the cyclic stability of TiNiPdCu-based high-temperature shape memory alloys.* Acta Materialia, 2013. **61**(13): p. 4797-4810.

23. Hartl, D.J., et al., *Use of a Ni60Ti shape memory alloy for active jet engine chevron application: I. Thermomechanical characterization.* Smart Materials & Structures, 2010. **19**(1).

24. Casciati, F., et al., *Fatigue Damage Accumulation in a Cu-based Shape Memory Alloy: Preliminary Investigation.* Cmc-Computers Materials & Continua, 2011. **23**(3): p. 287-306.

25. Birman, V., *Effect of SMA dampers on nonlinear vibrations of elastic structures.*, in *SPIE. 3038. 268 - 276*. 1997. p. 268 - 276.

26. Qian, H., et al., *Recentering shape memory alloy passive damper for structural vibration control.* Mathematical problems in engineering, 2013. **2013**: p. 13 pages.

27. Ma, H.W. and C.D. Cho, *Feasibility study on a superelastic SMA damper with re-centring capability.* Materials science and engineering A - structural materials properties microstructure and processing, 2008. **473**(1-2): p. 290-296.

28. van de Lindt, J.W. and A. Potts, *Shake table testing of a superelastic shape memory alloy response modification device in a wood shearwall.* Journal of structural engineering-Asce, 2008. **134**(8): p. 1343-1352.

29. Zuo, X.B. and A.Q. Li, *Numerical and experimental investigation on cable vibration mitigation using shape memory alloy damper.* Structural Control & Health Monitoring, 2011. **18**(1): p. 20-39.

30. Parulekar, Y.M., et al., *Seismic response attenuation of structures using shape memory alloy dampers.* Structural Control & Health Monitoring, 2012. **19**(1): p. 102-119.

31. Liang, C. and C.A. Rogers, *Design of shape memory alloy springs with applications in vibration control.* Journal of intelligent material systems and structures, 1997. **8**(4): p. 314-322.

32. Saadat, S., et al., *An overview of vibration and seismic applications of NiTi shape memory alloy.* Smart materials & structures, 2002. **11**(2): p. 218-229.

33. Belyaev, S.P., A.E. Volkov, and A.V. Voronkov, *Mechanical oscillations in TiNi under synchronized martensite transformations.* Journal of Engineering Materials and Technology-Transactions of the Asme, 1999. **121**(1): p. 105-107.

34. Williams, K., G. Chiu, and R. Bernhard, *Adaptive-passive absorbers using shape-memory alloys.* Journal of sound and vibration, 2002. **249**(5): p. 835-848.

35. Rustighi, E., M.J. Brennan, and B.R. Mace, *A shape memory alloy adaptive tuned vibration absorber: design and implementation.* Smart materials & structures, 2005. **14**(1): p. 19-28.

36. Araki, Y., et al., *Potential of superelastic Cu-Al-Mn alloy bars for seismic applications.* Earthquake Engineering & Structural Dynamics, 2011. **40**(1): p. 107-115.

37. Araki, Y., et al., *Rate-dependent response of superelastic Cu-Al-Mn alloy rods to tensile cyclic loads.* Smart Materials and Structures, 2012. **21**(3).

38. Araki, Y., et al., *Integrated mechanical and material design of quasi-zero-stiffness vibration isolator with superelastic Cu-Al-Mn shape memory alloy bars.* Journal of Sound and Vibration, 2015. **358**: p. 74-83.

39. Araki, Y., et al., *Feasibility of tension braces using Cu-Al-Mn superelastic alloy bars.* Structural Control & Health Monitoring, 2014. **21**(10): p. 1304-1315.

40. Hosseini, F., et al., *An experimental investigation of innovative bridge columns with engineered cementitious composites and Cu-Al-Mn super-elastic alloys.* Smart Materials and Structures, 2015. **24**(8).

41. Zieliński, T.P. and K. Duda, *Frequency and damping estimation methods - an overview.* Metrology and measurement systems, 2011. **18**(4): p. 505 - 528.

42. Sarkar, T.K. and O. Pereira, *Using the Matrix Pencil Method to Estimate the Parameters of a Sum of Complex Exponentials.* Ieee antennas and propagation magazine, 1995. **37**(1): p. 48-55.

43. Gencturk, B., et al., *Loading rate and temperature dependency of superelastic Cu–Al–Mn alloys.* Construction and building materials, 2014. **53**: p. 555 - 560.

44. Torra, V., et al., *Shape memory alloys: From the physical properties of metastable phase transitions to dampers for civil engineering applications.* Journal de physique Iv, 2004. **113**: p. 85-90.

45. Strnadel, B., et al., *Cyclic stress-strain characteristics of Ti-Ni and Ti-Ni-Cu shape-memory alloys.* Materials science and engineering a-structural materials properties microstructure and processing, 1995. **202**(1-2): p. 148-156.

46. Niitsu, K., T. Omori, and R. Kainuma, *Superelasticity at low temperatures in Cu-17Al-15Mn (at%) shape memory alloy.* Materials transactions, 2011. **52**(8): p. 1713-1715.

47. Nemat-Nasser, S., et al., *High strain-rate, small strain response of a NiTi shape-memory alloy.* Journal of engineering materials and technology-transactions of the asme, 2005. **127**(1): p. 83-89.

48. Priestley, M.J.N., F. Seible, and G.M. Calvi, *Seismic design and retrofit of bridges.* 1996, New York: John Wiley. xvii, 686 p.

49. Connor, J.J., *Introduction to structural motion control*. MIT-Prentice Hall series on civil, environmental, and systems engineering. 2003, Upper Saddle River, N.J.: Prentice Hall Pearson Education, Inc. xiv, 680 p.

50. Schmitz, T.L. and K.S. Smith, *Mechanical vibrations modeling and measurement*. 2012, Springer Science+Business Media, LLC: New York, NY.

51. Adam, C. and T. Furtmuller, *Seismic Performance of Tuned Mass Dampers.* Mechanics and Model-Based Control of Smart Materials and Structures, 2010: p. 11-18.

52. Schmelzer, B., M. Oberguggenberger, and C. Adam, *Efficiency of tuned mass dampers with uncertain parameters on the performance of structures under stochastic excitation.* Proceedings of the Institution of Mechanical Engineers Part O-Journal of Risk and Reliability, 2010. **224**(O4): p. 297-308.

53. Casciati, F. and F. Giuliano, *Tuned mass dampers in the towers of suspension bridges.* Innovation in Computational Structures Technology, 2006: p. 439-473.

54. Nagarajaiah, S. and E. Sonmez, *Structures with semiactive variable stiffness single/multiple tuned mass dampers.* Journal of structural engineering-Asce, 2007. **133**(1): p. 67-77.

55. Xue, S., et al., *Natural frequency changes for damaged and reinforced real structure in comparison with shake table and simulation.* Materials forum, 2009. **33**: p. 344-350.

56. Pandey, A.K., M. Biswas, and M.M. Samman, *Damage detection from changes in curvature mode shapes.* Journal of sound and vibration, 1991. **145**(2): p. 321-332.

57. Luco, J.E., M.D. Trifunac, and H.L. Wong, *On the apparent change in dynamic behavior of a 9-story reinforced-concrete building.* Bulletin of the seismological society of america, 1987. **77**(6): p. 1961-1983.

58. Brincker, R., J. Rodrigues, and P. Andersen, *Scaling the mode shapes of a building model by mass changes*, in *IMAC-22: A Conference on Structural Dynamics*. 2004, Society for Experimental Mechanics: Hyatt Regency Dearborn, Dearborn, Michigan, USA. p. 119-126.

59. Meirovitch, L., *Fundamentals of vibrations*. 2001, Boston: McGraw-Hill. xviii, 806 p.

60. Connor, J., S. Laflamme, and SpringerLink (Online service), *Structural Motion Engineering*. 2014, Springer International Publishing,: S.l. p. 1 online resource.

61. Soul, H., et al., *Pseudoelastic fatigue of NiTi wires: frequency and size effects on damping capacity.* Smart Materials & Structures, 2010. **19**(8).

Table 1 Testing protocol for the cantilever beam-TMD system

	Main structure			TMD			
Test No.	m_1 (kg)[1]	f_1 (Hz)[2]	T (°C)[3]	k_2 (N/m)[4]	ξ_2 (%)[5]	m_2 (kg)[6]	f_2 (Hz)[7]
1	61.6	4.41	-	-	-	-	-
2	61.6	4.41	21	2704.76	0.81	3.6	4.38
3	71.5	4.02	-	-	-	-	-
4	71.5	4.02	21	2704.76	0.81	3.6	4.38
5	71.5	4.02	11	2282.19	1.84	3.6	4.03
6	54.1	4.74	-	-	-	-	-
7	54.1	4.74	21	2704.76	0.81	3.6	4.38
8	54.1	4.74	120	3192.96	0.20	3.6	4.76

[1] mass attached to the steel cantilever beam

[2] natural frequency of the main structure

[3] working temperature of the SMA beam

[4] stiffness of the SMA beam

[5] equivalent damping ratio of the SMA beam

[6] mass attached to the SMA beam

[7] natural frequency of the TMD

Dear Editor,

Please find table which we respond to all the comments that reviewer has, we have considered comments from reviewer, responded and amended our manuscript as appropriate. The comments from reviewer are very useful to improve the quality of the manuscript, his/her efforts and time are much appreciated. We are looking forward to working with you during the review process.

Best regards,

Wen-Shao Chang

Reviewer 2:

Reviewer's comments	Response to reviewer
According the MANDATORY remarks of the previous refereeing, suppress the figures 7-8-9. In fact, not includes clear recoverable data. If introduction of 3-D figures can be considered of potential interest but in this case this idea cannot be considered. Please suppress figures 7-8-9 and adapt the text.	We agree with the reviewer's comments. We have suppressed Figures 7-8-9 and adapted the relevant text.

1
2
3
4
5
6
7
8
9
10
11
12
13
14
15
16
17
18
19
20
21
22
23
24
25
26
27
28
29
30
31
32
33
34
35
36
37
38
39
40
41
42
43
44
45
46
47
48
49
50
51
52
53
54
55
56
57
58
59
60
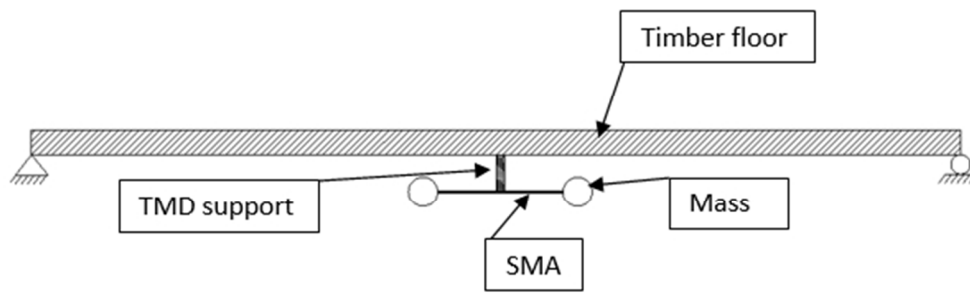
Figure 1 Timber floor using tuned mass damper by bending SMA
160x50mm (96 x 96 DPI)
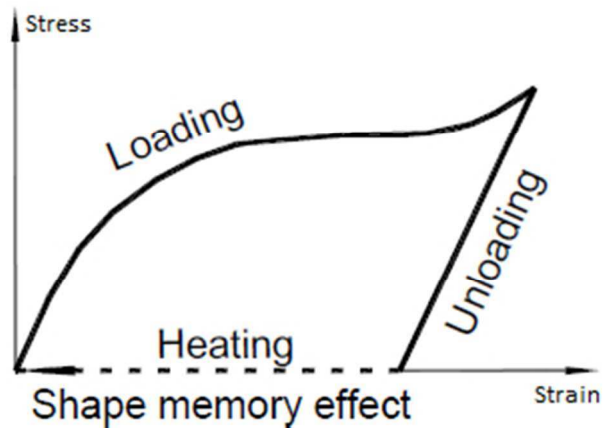
Figure 2 Stress-strain curve demonstrating the shape memory effect (left)
84x58mm (96 x 96 DPI)
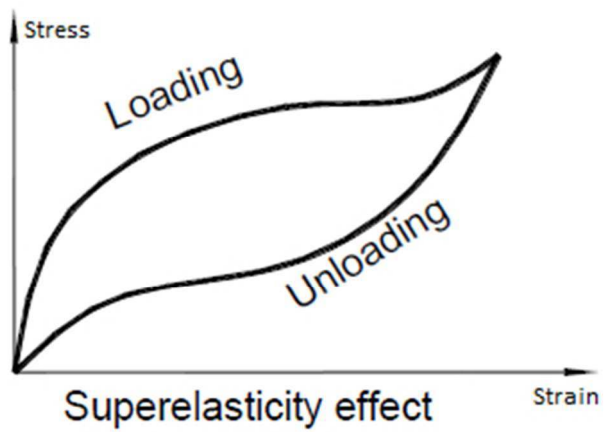
Figure 2 Stress-strain curve demonstrating the superelasticity (right)
84x59mm (96 x 96 DPI)

1
2
3
4
5
6
7
8
9
10
11
12
13
14
15
16
17
18
19
20
21
22
23
24
25
26
27
28
29
30
31
32
33
34
35
36
37
38
39
40
41
42
43
44
45
46
47
48
49
50
51
52
53
54
55
56
57
58
59
60
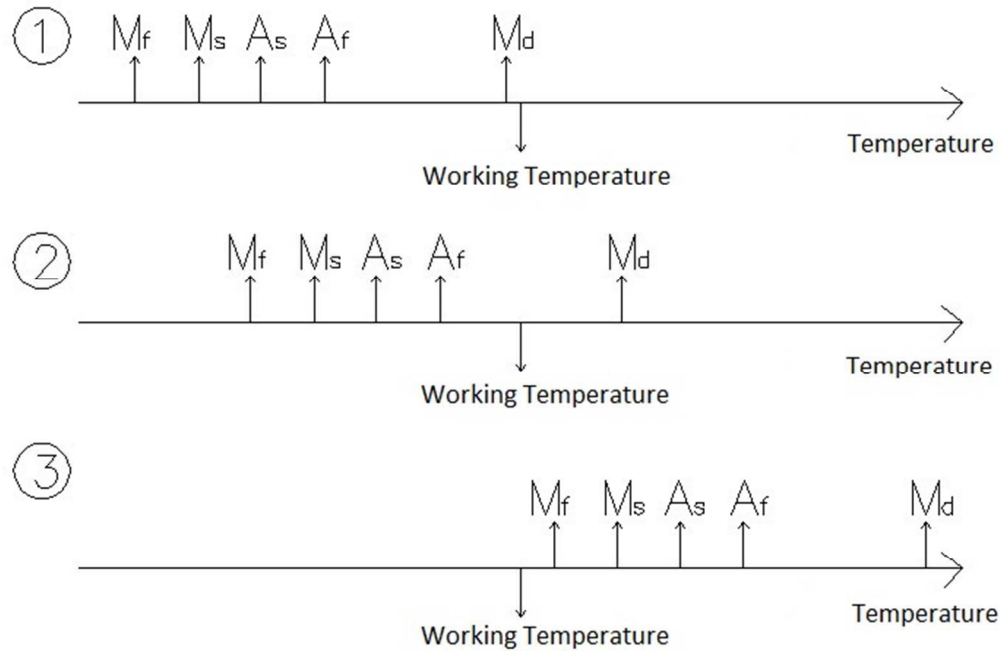
Figure 3 (1) Plastic deformation; (2) superelasticity; (3) shape memory effect
181x118mm (96 x 96 DPI)

Figure 4 (a) Cu-Al-Mn SMA vibration sample
238x136mm (96 x 96 DPI)
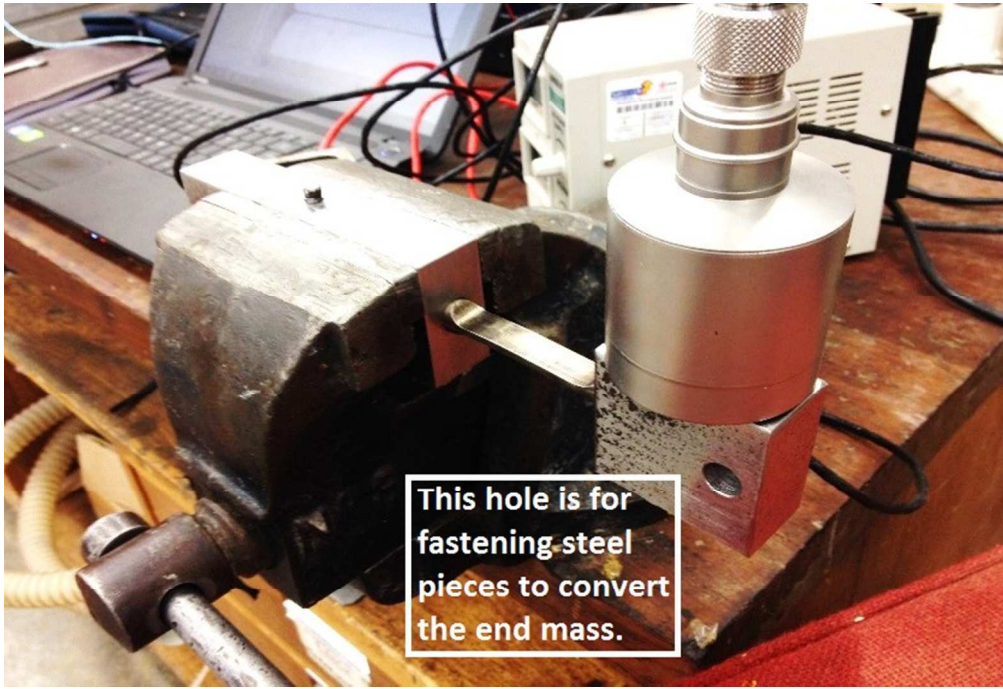
Figure 4 (b) SMA free vibration test set-up
95x65mm (220 x 220 DPI)
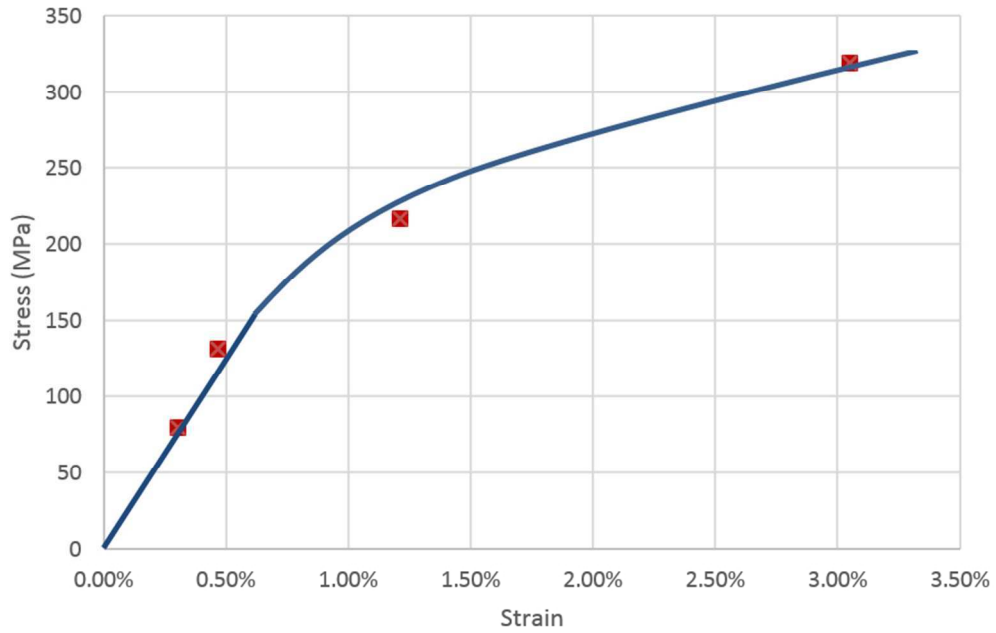
Figure 5 Static strain-stress graph of SMA cantilever beam
238x156mm (96 x 96 DPI)
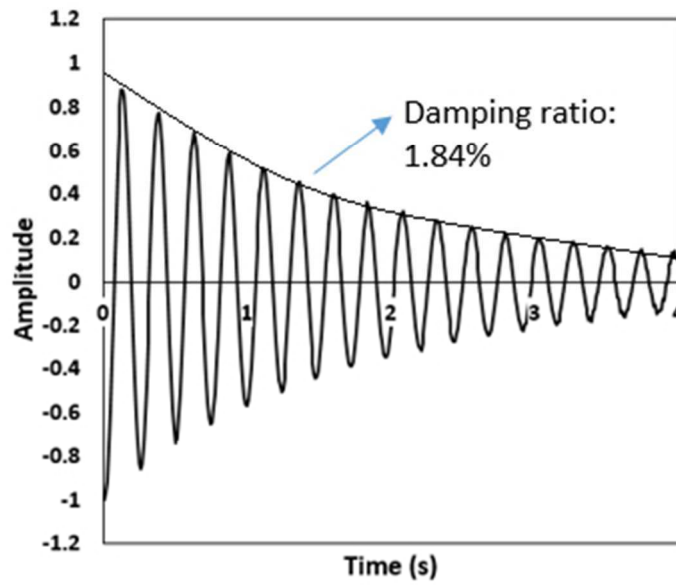
Figure 6 Normalised free vibration response at pre-stress level of 216 MPa in first 4 seconds (a) at 11℃
94x78mm (96 x 96 DPI)

Figure 6 Normalised free vibration response at pre-stress level of 216 MPa in first 4 seconds (b) at 80℃
98x80mm (96 x 96 DPI)

1
2
3
4
5
6
7
8
9
10
11
12
13
14
15
16
17
18
19
20
21
22
23
24
25
26
27
28
29
30
31
32
33
34
35
36
37
38
39
40
41
42
43
44
45
46
47
48
49
50
51
52
53
54
55
56
57
58
59
60
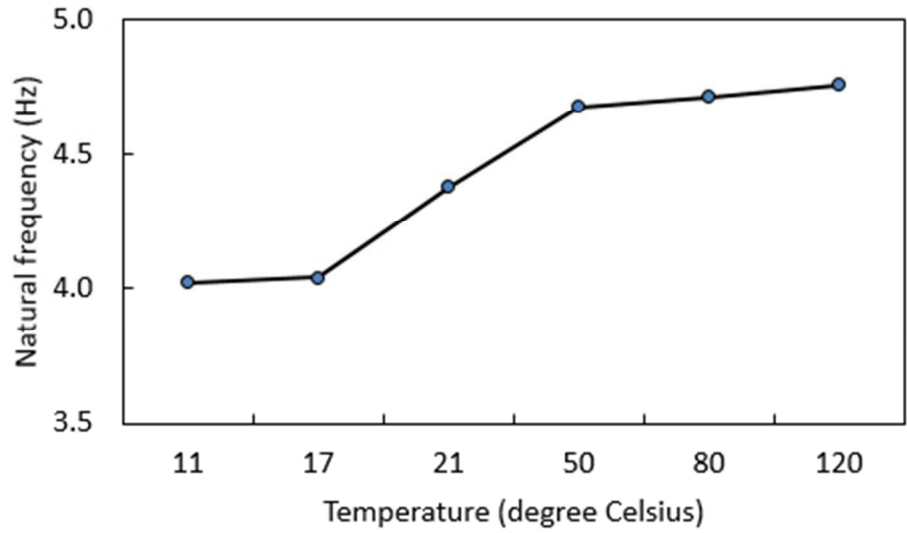
Figure 7 Effect of temperature on the natural frequency of SMA cantilever beam at pre-stress level of 216MPa
121x72mm (96 x 96 DPI)
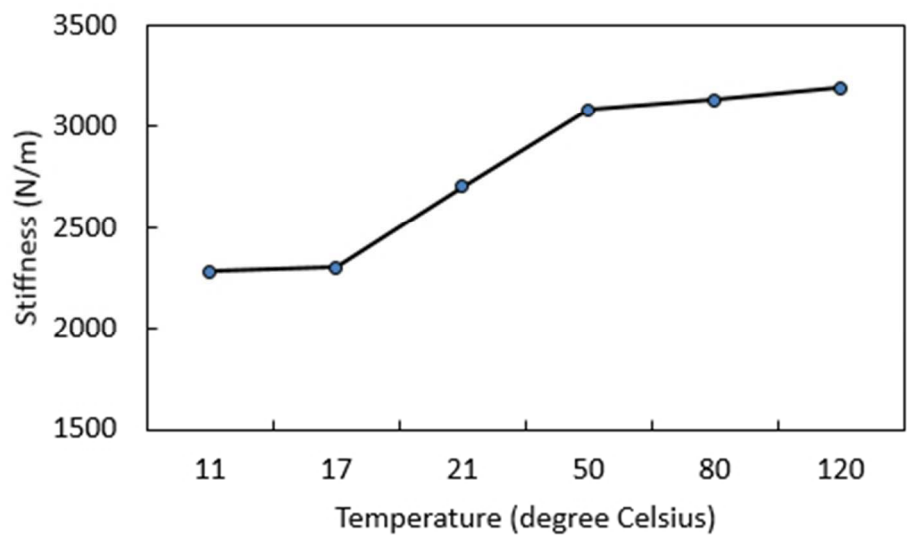
Figure 8 Effect of temperature on the equivalent stiffness of SMA cantilever beam at pre-stress level of
216MPa
123x72mm (96 x 96 DPI)
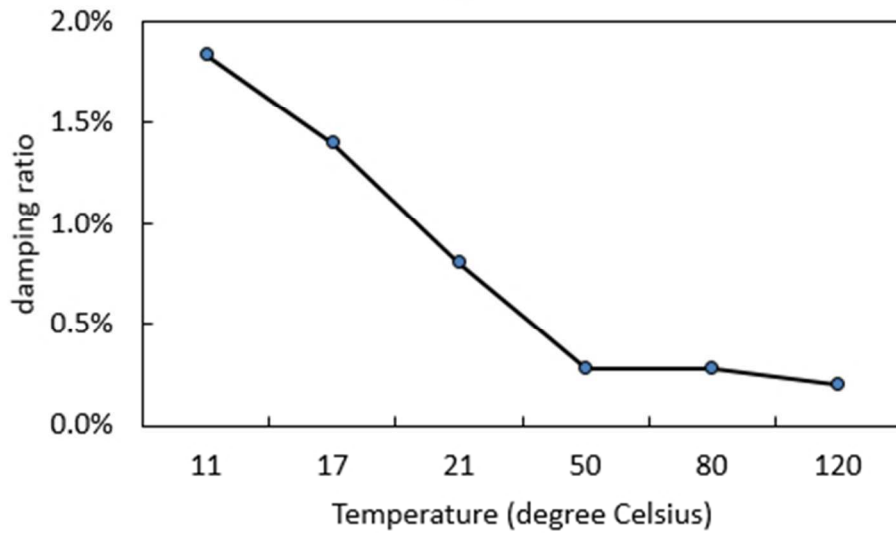
Figure 9 Effect of temperature on the damping ratio of SMA cantilever beam at pre-stress level of 216MPa
122x73mm (96 x 96 DPI)

1
2
3
4
5
6
7
8
9
10
11
12
13
14
15
16
17
18
19
20
21
22
23
24
25
26
27
28
29
30
31
32
33
34
35
36
37
38
39
40
41
42
43
44
45
46
47
48
49
50
51
52
53
54
55
56
57
58
59
60
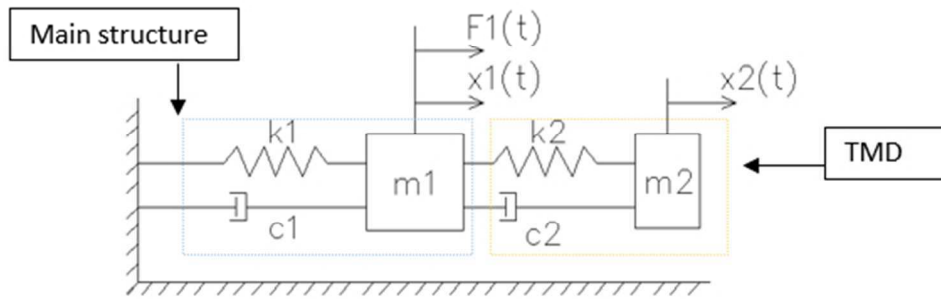
Figure 10 Idealisation of the timber floor system with TMD
157x55mm (96 x 96 DPI)

1
2
3
4
5
6
7
8
9
10
11
12
13
14
15
16
17
18
19
20
21
22
23
24
25
26
27
28
29
30
31
32
33
34
35
36
37
38
39
40
41
42
43
44
45
46
47
48
49
50
51
52
53
54
55
56
57
58
59
60
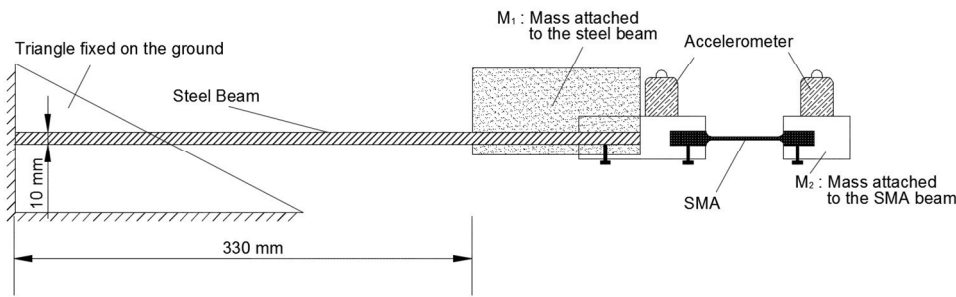
Figure 11 Schematic drawing of the experimental set-up
413x143mm (96 x 96 DPI)
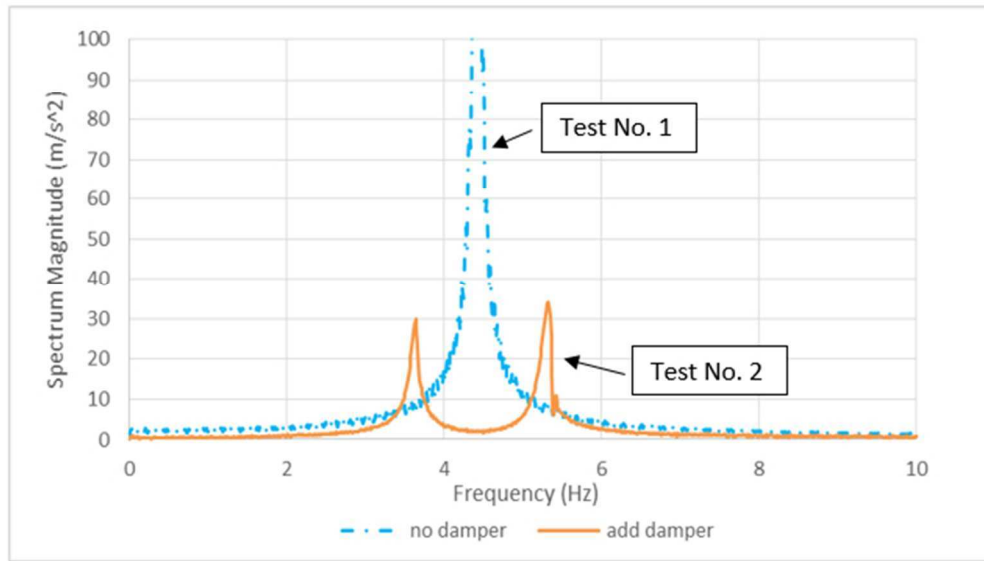
Figure 12 Frequency response of cantilever beam without and with damper (m_1=61.6 kg)
169x97mm (96 x 96 DPI)

1
2
3
4
5
6
7
8
9
10
11
12
13
14
15
16
17
18
19
20
21
22
23
24
25
26
27
28
29
30
31
32
33
34
35
36
37
38
39
40
41
42
43
44
45
46
47
48
49
50
51
52
53
54
55
56
57
58
59
60
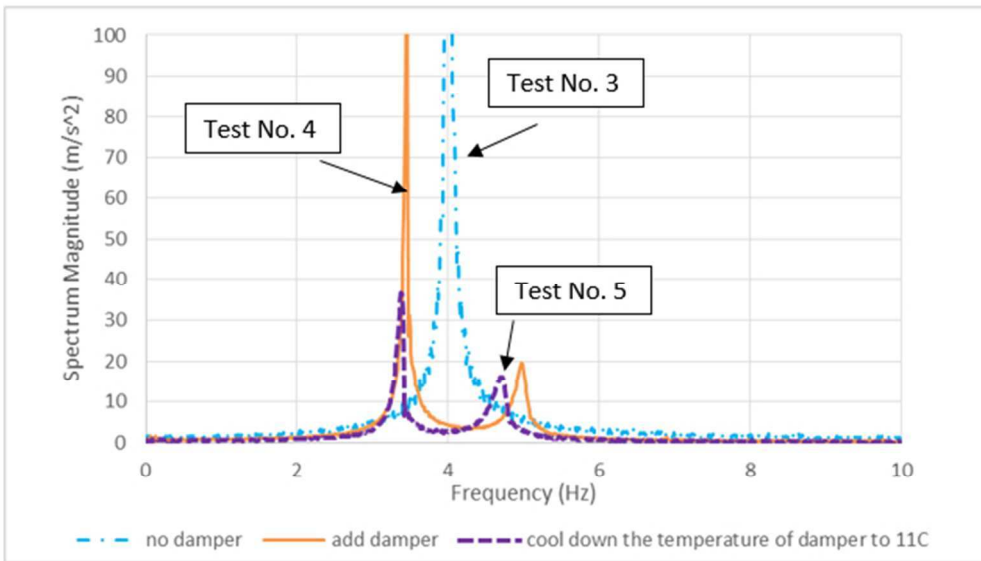
Figure 13 Frequency response of cantilever beam without damper, with damper and with temperature controlled damper (m_1=71.5 kg)
169x97mm (96 x 96 DPI)
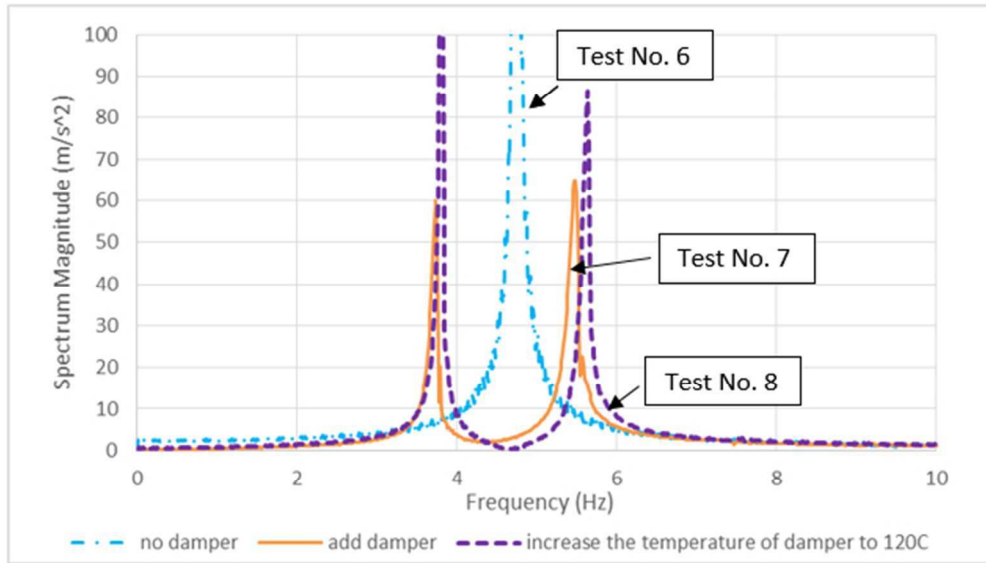
Figure 14 Frequency response of the cantilever beam without damper, with damper and with temperature controlled damper (m_1=54.1 kg)
168x97mm (96 x 96 DPI)